






ORIGINAL ARTICLE

Synthesis of new two-dimensional titanium carbonitride $\text{Ti}_2\text{C}_{0.5}\text{N}_{0.5}\text{T}_x$ MXene and its performance as an electrode material for sodium-ion battery

Kun Liang¹  | Anika Tabassum¹ | Ahmad Majed¹ | Chaochao Dun²  | Feipeng Yang³  | Jinghua Guo³ | Kaitlyn Prenger¹  | Jeffrey J. Urban² | Michael Naguib¹ 

¹Department of Physics and Engineering Physics, Tulane University, New Orleans, Louisiana, USA

²The Molecular Foundry, Lawrence Berkeley National Laboratory, Berkeley, California, USA

³Advanced Light Source, Lawrence Berkeley National Laboratory, Berkeley, California, USA

Correspondence

Michael Naguib, Department of Physics and Engineering Physics, Tulane University, New Orleans, LA 70118, USA. Email: naguib@tulane.edu

Funding information

Fluid Interface Reactions, Structures and Transport (FIRST) Center, an Energy Frontier Research Center funded by the U.S. Department of Energy, Office of Science, Office of Basic Energy Sciences

Abstract

Two-dimensional (2D) layered transition metal carbides/nitrides, called MXenes, are attractive alternative electrode materials for electrochemical energy storage. Owing to their metallic electrical conductivity and low ion diffusion barrier, MXenes are promising anode materials for sodium-ion batteries (SIBs). Herein, we report on a new 2D carbonitride MXene, *viz.*, $\text{Ti}_2\text{C}_{0.5}\text{N}_{0.5}\text{T}_x$ (T_x stands for surface terminations), and the only second carbonitride after Ti_3CNT_x so far. A new type of *in situ* HF (HCl/KF) etching condition was employed to synthesize multilayer $\text{Ti}_2\text{C}_{0.5}\text{N}_{0.5}\text{T}_x$ powders from $\text{Ti}_2\text{AlC}_{0.5}\text{N}_{0.5}$. Spontaneous intercalation of tetramethylammonium followed by sonication in water allowed for large-scale delamination of this new titanium carbonitride into 2D sheets. Multilayer $\text{Ti}_2\text{C}_{0.5}\text{N}_{0.5}\text{T}_x$ powders showed higher specific capacities and larger electroactive surface area than those of Ti_2CT_x powders. Multilayer $\text{Ti}_2\text{C}_{0.5}\text{N}_{0.5}\text{T}_x$ powders show a specific capacity of 182 mAh g^{-1} at 20 mA g^{-1} , the highest among all reported MXene electrodes as SIBs with excellent cycling stability.

KEYWORDS

MXene, sodium-ion battery, titanium carbonitride, two-dimensional

1 | INTRODUCTION

MXenes are two-dimensional (2D) transition metal carbides and/or nitrides with a composition of $\text{M}_{n+1}\text{X}_n\text{T}_x$, where M represents an early transition metal (*e.g.*, Ti, V, Cr, Nb, Mo), X is C and/or N, n can be 1–4, and T_x

denotes the surface terminations.^{1–3} Most MXenes are synthesized by selective etching of atomically thin layers from layered transition metal carbides and nitrides called MAX phases.¹ Several etchants can be used to synthesize MXenes such as aqueous hydrofluoric acid (HF),⁴ *in situ* HF using a mixture of aqueous acid and fluoride salts,⁵ hydrolyzed ionic liquids,⁶ and molten salts.⁷ The surface of as-synthesized MXene is terminated by the mixture of moieties such as O, OH, F, Cl, I, Br, and so forth.⁸

Kun Liang and Anika Tabassum authors contributed equally to this work.

This is an open access article under the terms of the Creative Commons Attribution License, which permits use, distribution and reproduction in any medium, provided the original work is properly cited.

© 2021 The Authors. *InfoMat* published by UESTC and John Wiley & Sons Australia, Ltd.

In addition to their large compositional space, MXenes offer unique properties compared with other 2D materials. For example, MXenes demonstrate metallic electrical conductivity (up to $\sim 24\,000\text{ S cm}^{-1}$ for $\text{Ti}_3\text{C}_2\text{T}_x$),⁹ hydrophilicity,² and high strength.¹⁰ These unique properties combined with rich surface chemistry and the capability to host ions promoted MXenes for many applications ranging from electrochemical energy storage,^{11–14} to sensing,^{12,15} water purification,¹⁶ and catalysis.^{17–19}

One of the great advantages of MXenes is their tunability, as tuning their compositions allows for optimizing their properties and performance. Most of the efforts for such tuning have been focused on tuning the M in MXene by introducing more than one transition metal at the M site, forming ordered double transition metals or solid solution MXenes.^{20–24} Another parameter that has been explored is controlling the surface terminations, which has been proven to be an effective means to control the properties of MXenes.^{25,26} To date, over 40 different MXene compositions have been reported; the vast majority of these MXenes are carbides with only a few exceptions—several nitrides and only one carbonitride (*viz.*, Ti_3CNT_x).²⁷ The latter has shown distinct properties and behavior compared with $\text{Ti}_3\text{C}_2\text{T}_x$ in many applications including energy storage,^{28–33} optics,^{34,35} catalysis,^{36–39} electromagnetic shielding,^{40,41} sensing,^{42,43} and so forth. This distinct behavior of Ti_3CNT_x compared with $\text{Ti}_3\text{C}_2\text{T}_x$ provides a strong motivation to develop other new carbonitrides to join the MXene family. Also, computational calculations predict that introducing N into $\text{Ti}_3\text{C}_2\text{T}_x$ will increase the number of electrons and provide more active sites for Na^+ , making carbonitride a promising anode material for sodium-ion batteries (SIBs).⁴⁴ For example, Zhu *et al.* reported the use of Ti_3CNT_x as an anode material for SIBs to deliver a higher specific capacity than that of $\text{Ti}_3\text{C}_2\text{T}_x$.³⁰ Since Ti_2CT_x ($n = 1$) outperforms $\text{Ti}_3\text{C}_2\text{T}_x$ ($n = 2$) when tested in SIBs and Na-ion capacitors,^{45,46} it is reasonable to predict that $\text{Ti}_2\text{C}_{0.5}\text{N}_{0.5}\text{T}_x$ would exhibit a better electrochemical performance than both Ti_3CNT_x and Ti_2CT_x . Moreover, the computational structural, electronic, mechanical, and lattice dynamical properties were reported in the literature;⁴⁷ therefore, $\text{Ti}_2\text{C}_{0.5}\text{N}_{0.5}\text{T}_x$ would be a promising MXene material for different applications.

One of the reasons for the limited number of nitride and carbonitride MXenes is the lower stability of nitride-based MXenes compared with their carbide counterparts.⁴⁸ This renders their synthesis a challenging task because they tend to dissolve/oxidize in the etching solution.⁴⁹ Therefore, careful selection of the synthesis approach is necessary to realize new carbonitride MXenes.

Herein, we report the synthesis of a pure $\text{Ti}_2\text{AlC}_{0.5}\text{N}_{0.5}$ MAX phase and its exfoliation into $\text{Ti}_2\text{C}_{0.5}\text{N}_{0.5}$

T_x (T_x indicates surface terminations) MXene, which is a new member of MXene family, and the only second carbonitride after Ti_3CNT_x . In this work, we summarize the protocol to prepare $\text{Ti}_2\text{AlC}_{0.5}\text{N}_{0.5}$ MAX phase, multilayer $\text{Ti}_2\text{C}_{0.5}\text{N}_{0.5}\text{T}_x$ powders, and mono-/few-layer $\text{Ti}_2\text{C}_{0.5}\text{N}_{0.5}\text{T}_x$ 2D sheets, including a new type of *in situ* HF (HCl/KF) etching condition. In addition, we investigated the electrochemical performance and kinetics of multilayer $\text{Ti}_2\text{C}_{0.5}\text{N}_{0.5}\text{T}_x$ powders as an anode material in SIBs. Multilayer $\text{Ti}_2\text{C}_{0.5}\text{N}_{0.5}\text{T}_x$ powders show higher specific capacities with a larger electroactive surface area than those of Ti_2CT_x powders prepared using the same approach, which agrees with reported theoretical predictions. Multilayer $\text{Ti}_2\text{C}_{0.5}\text{N}_{0.5}\text{T}_x$ powders show a specific capacity of 182 mAh g^{-1} at 20 mA g^{-1} , the highest of all reported multilayer MXenes as SIB electrodes and excellent cycling stability. The introduced new member of MXenes and its noteworthy excellent electrochemical performance open up a more fundamental understanding to the unique structures of MXenes and their related applications in the field of renewable energy.

2 | RESULTS AND DISCUSSION

X-ray diffraction (XRD) patterns of $\text{Ti}_2\text{AlC}_{0.5}\text{N}_{0.5}$ MAX phase, $\text{Ti}_2\text{C}_{0.5}\text{N}_{0.5}\text{T}_x$ multilayer MXene powder, and free-standing delaminated MXene paper are shown in Figure 1A. The as-prepared $\text{Ti}_2\text{AlC}_{0.5}\text{N}_{0.5}$ phase XRD pattern agrees with the reported literature, which confirms the successful synthesis of a predominantly single-phase $\text{Ti}_2\text{AlC}_{0.5}\text{N}_{0.5}$.^{50,51} To prepare $\text{Ti}_2\text{C}_{0.5}\text{N}_{0.5}\text{T}_x$ MXene, we first attempted using aqueous HF etching, but observed huge weight loss even at concentrations as low as 10% (more details can be found in Supporting Information, Figure S1, and Table S1), so we switched our efforts to an *in situ* HF etching method, which is milder than the traditional HF. Thus, in the present work, an HCl/KF mixture was used to etch the MAX phase. The rationale behind using KF, instead of the LiF traditionally used in the *in situ* HF synthesis of MXene, is the fact that KF is water-soluble, and therefore fluoride salt impurities in the multilayer MXene powder can be avoided, unlike that in the case of LiF. Compared with pristine MAX phase, the (002) peak became broad and shifted to a lower angle, indicating the successful removal of Al from layered $\text{Ti}_2\text{AlC}_{0.5}\text{N}_{0.5}$ and full conversion into MXene.⁵² The (002) peak shifted from a 2θ of 13.13° for MAX phase to 7.42° after etching, which suggests an expansion of the interlayer distance (d -spacing) from 6.8 to 11.9 Å from MAX phase to multilayer $\text{Ti}_2\text{C}_{0.5}\text{N}_{0.5}\text{T}_x$ MXene. Large expansion in d -spacing

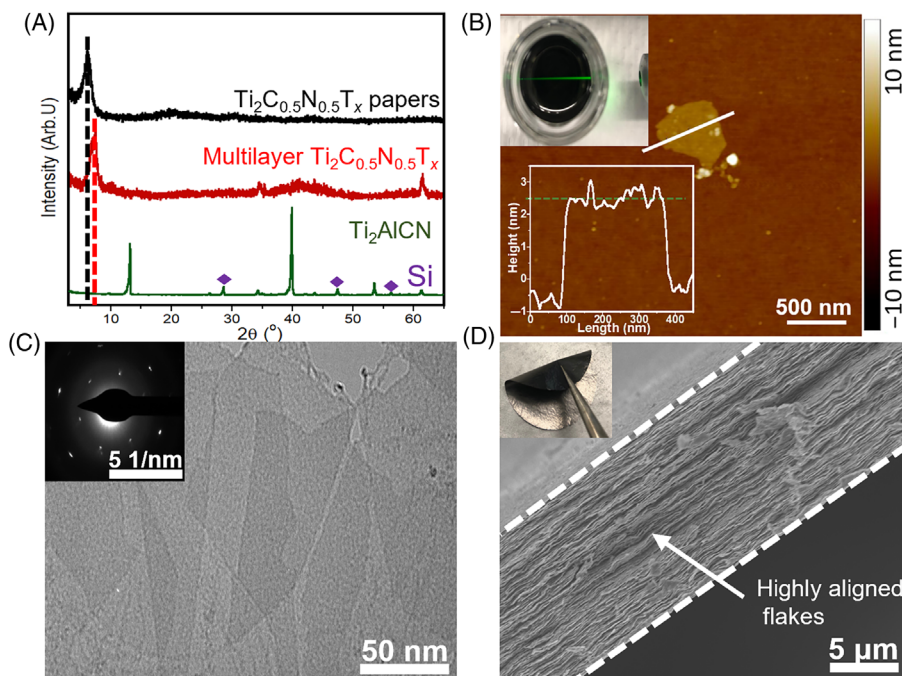


FIGURE 1 Morphological and structural characterizations of $\text{Ti}_2\text{C}_{0.5}\text{N}_{0.5}\text{T}_x$ MXene. (A) X-ray diffraction patterns of pristine $\text{Ti}_2\text{AlC}_{0.5}\text{N}_{0.5}$ MAX phase (green pattern), multilayer $\text{Ti}_2\text{C}_{0.5}\text{N}_{0.5}\text{T}_x$ MXene (red pattern), and freestanding $\text{Ti}_2\text{C}_{0.5}\text{N}_{0.5}\text{T}_x$ MXene papers (black pattern). The diamond symbols represent the peak positions for Si that was added as an internal reference in the MAX phase sample. (B) Atomic force microscopy image of $\text{Ti}_2\text{C}_{0.5}\text{N}_{0.5}\text{T}_x$ flakes deposited on a silicon wafer. The inset at the top left is a photograph of a colloidal solution of delaminated $\text{Ti}_2\text{C}_{0.5}\text{N}_{0.5}\text{T}_x$ after centrifuging, showing the Tyndall effect. The inset at the bottom left is the height profile along the solid white line. (C) TEM image of delaminated $\text{Ti}_2\text{C}_{0.5}\text{N}_{0.5}\text{T}_x$ 2D sheets. The inset is an selected area electron diffraction pattern, showing hexagonal symmetry. (D) Cross-sectional scanning electron microscopy image of a freestanding $\text{Ti}_2\text{C}_{0.5}\text{N}_{0.5}\text{T}_x$ paper. A photograph of the same paper but bent and held using tweezers is shown as inset in (D)

from MAX to MXene can be explained by intercalation of cations, water, and/or etching products (e.g., AlF_x).^{53,54} The successful etching of Al from the MAX phases and its replacement with O and F were confirmed using energy dispersive X-ray spectroscopy (EDS) (Table S2).

The scanning electron microscopy (SEM) images of MAX and multilayer $\text{Ti}_2\text{C}_{0.5}\text{N}_{0.5}\text{T}_x$ MXene are shown in Figure S2. The lack of accordion-like morphology in the $\text{Ti}_2\text{C}_{0.5}\text{N}_{0.5}\text{T}_x$ (Figure S2B), which is commonly observed for HF synthesized MXenes,^{2,4} after HCl/KF etching is in agreement with what was reported by Ghidui *et al.*⁵ for HCl/LiF etching of Ti_3AlC_2 and is explained by cation and/or water intercalation.

Unlike HCl/LiF etching of Ti_3AlC_2 , when we attempted to delaminate the multilayer MXene by sonication in water, the yield was extremely small. This may be explained by the low K content after etching (Table S2) that was only about 0.02 for each 2Ti. Thus, to achieve large-scale delamination, we soaked the multilayer MXene powders in tetramethylammonium hydroxide (TMAOH) to intercalate large TMA^+ cations and induce a significant layer expansion, therefore overcoming any hydrogen and van der Waals bonding

between the layers.^{55,56} After intercalation, washing was carried out to remove excess TMAOH and then the TMA intercalated MXene was sonicated in DI water followed by centrifuging. The supernatant was a black ink of delaminated MXene in water. As shown in the inset of Figure 1B, a clear Tyndall effect can be observed in the diluted colloidal solution after centrifuging, confirming dispersion of nanomaterials in water. The atomic force microscopy (AFM) image (Figure 1B) shows a nanoflake with a thickness of ~ 2.5 nm (~ 2 – 3 layers),⁵⁷ evidencing the formation of few-layer $\text{Ti}_2\text{C}_{0.5}\text{N}_{0.5}\text{T}_x$ MXene. Transmission electron microscopy (TEM) (Figure 1C) shows many overlapping 2D sheets of $\text{Ti}_2\text{C}_{0.5}\text{N}_{0.5}\text{T}_x$. Both AFM and TEM confirm the successful delamination of multilayer MXene into single- and few-layer MXene. The selected area electron diffraction (SAED) pattern (Figure 1C, inset) confirms the hexagonal symmetry of the planes, suggesting that MXene maintains the hexagonal basal plane structure of the parent MAX phase. Filtering the colloidal solution of delaminated MXene resulted in a freestanding paper shown in the inset of Figure 1D. The morphology of the highly aligned restacked flakes

can be seen in the cross-sectional SEM image in Figure 1D. The electrical conductivity of the as-prepared free-standing $\text{Ti}_2\text{C}_{0.5}\text{N}_{0.5}\text{T}_x$ paper with a thickness of $2.5\ \mu\text{m}$ is $\sim 435 \pm 25\ \text{S cm}^{-1}$, which is higher than that of Ti_2CT_x ($\sim 354 \pm 50\ \text{S cm}^{-1}$) using the same procedures, but lower than those of Ti_3CNT_x and Ti_2CT_x using other *in situ* HF methods.^{58,59} This is the first work to report the new MXene, $\text{Ti}_2\text{C}_{0.5}\text{N}_{0.5}\text{T}_x$, but we believe that the conductivity can be improved significantly by further development and optimization of different etching/delamination methods similar to what was reported for $\text{Ti}_3\text{C}_2\text{T}_x$.⁹

X-ray photoelectron spectroscopy (XPS) measurements were conducted to analyze the chemical states of the elements. From the XPS survey of multilayer MXene in Figure S3, Ti, C, and N were detected with the terminating elements of O, F, and Cl. A weak peak for Al indicates the removal of Al to form multilayer MXene, in agreement with EDS and XRD. As depicted in Figure 2A, Ti 2p was deconvoluted to +1, +2, +3, and +4 oxidation states, bonding to $-\text{O}/-\text{OH}/-\text{Cl}$ terminations. Exactly 24.5% photoemission of TiO_2 , coming from O-terminated MXene surface, is noted in the Ti 2p region, which is larger than that of Ti_2CT_x ,⁶⁰ reflecting that $\text{Ti}_2\text{C}_{0.5}\text{N}_{0.5}\text{T}_x$ MXene is more prone to oxidation than Ti_2CT_x MXene.

To further investigate the oxidation state of Ti in $\text{Ti}_2\text{C}_{0.5}\text{N}_{0.5}\text{T}_x$ MXene, X-ray absorption spectroscopy (XAS) measurement was conducted. Figure 2B shows the Ti L-edges XAS in total electron yield (TEY) mode, for Ti_2AlC , $\text{Ti}_2\text{AlC}_{0.5}\text{N}_{0.5}$, and their corresponding MXenes. While both MAX phases have comparable Ti L-edge profiles, it can be clearly observed that the Ti L-edge energy of $\text{Ti}_2\text{C}_{0.5}\text{N}_{0.5}\text{T}_x$ MXene moves slightly to a higher energy side compared with that of Ti_2CT_x MXene, indicating a higher average for Ti oxidation state in $\text{Ti}_2\text{C}_{0.5}\text{N}_{0.5}\text{T}_x$ MXene than that of Ti_2CT_x MXene. This is consistent with the reported theoretical results showing a lower stability of carbonitrides relative to their carbide counterparts.^{42,43} In addition, the bonding of $\text{TiO}_{2-x}\text{F}_x$ and $\text{CN}-\text{Ti}-\text{F}_x$ are located at higher binding energy regions because of the highly electronegative from F atom.⁶¹ From the C 1s peak in Figure 2C, we can see a clear Ti-CN peak, demonstrating the existence of titanium carbonitride. Shown in Figure 2D is a high-resolution scan of the N 1s region, which can be fitted to four peaks: $\text{CN}-\text{Ti}-\text{T}_x$ (396.84 eV), $\text{CN}-\text{Ti}-\text{F}$ (397.52 eV), $-\text{NR}_2/\text{N}-\text{O}$ (399.72 eV), and $\text{N}-\text{TiO}_x$ (401.28 eV). The binding energy of the latter three peaks is comparable with the reported N 1s peaks of Ti_3CNT_x .³⁵ For the O 1s peak in Figure S4A, it is notable that the O-termination is dominant. The detected K 2p in

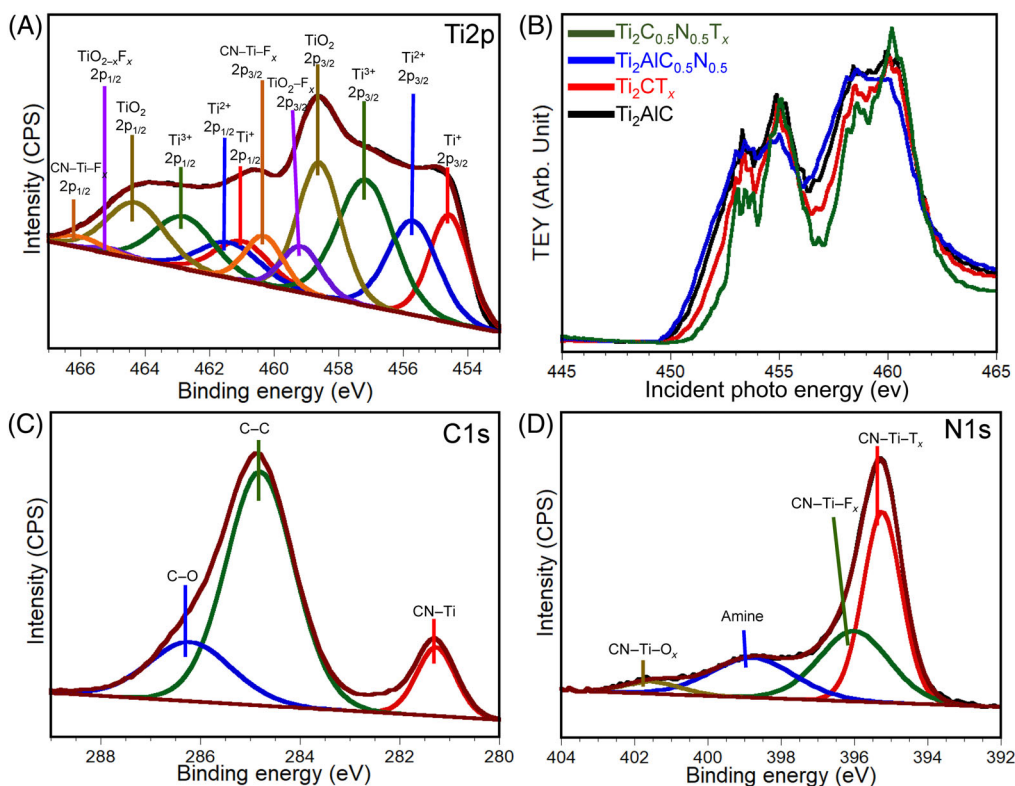


FIGURE 2 (A) High-resolution XPS spectra of Ti 2p in multilayer $\text{Ti}_2\text{C}_{0.5}\text{N}_{0.5}\text{T}_x$ MXene. (B) Ti L-edges in total electron yield (TEY) mode, for Ti_2AlC , $\text{Ti}_2\text{AlC}_{0.5}\text{N}_{0.5}$, and their corresponding MXenes. (C,D) High-resolution XPS spectra of C 1s and N 1s in multilayer $\text{Ti}_2\text{C}_{0.5}\text{N}_{0.5}\text{T}_x$ MXene, respectively

Figure S4E can be attributed to K intercalation into the layers during the etching process. More XPS details are presented in Figure S4 and Table S3.

To evaluate the electrochemical performance of $\text{Ti}_2\text{C}_{0.5}\text{N}_{0.5}\text{T}_x$ MXene in SIBs, standard CR 2032 coin cells were assembled with $\text{Ti}_2\text{C}_{0.5}\text{N}_{0.5}\text{T}_x$ MXene as a working electrode and Na foil as counter and reference electrodes in 1 M $\text{NaPF}_6/\text{EC-DEC}$ electrolyte. The cyclic voltammograms (CV) of $\text{Ti}_2\text{C}_{0.5}\text{N}_{0.5}\text{T}_x$ (Figure 3A) are different than those reported for Ti_2CT_x , $\text{Ti}_3\text{C}_2\text{T}_x$, and Ti_3CNT_x .^{30,45,62,63} This suggests that the partial replacement of C by N plays an important role in the electrochemical performance of MXene. Since recent reports suggest that synthesis conditions affect the electrochemical behavior of the same MXene,⁶⁴ for a more meaningful comparison, Ti_2CT_x was prepared using the same synthesis conditions as the newly synthesized $\text{Ti}_2\text{C}_{0.5}\text{N}_{0.5}\text{T}_x$. Not surprisingly,

as shown in Figure S5, we do not observe any of the peaks as found in the CV of Ti_2CT_x , and the shapes between $\text{Ti}_2\text{C}_{0.5}\text{N}_{0.5}\text{T}_x$ and Ti_2CT_x are similar, demonstrating the electrochemical behavior is similar. From the CV curves in Figure 3A, we can find broad peaks, without clearly separated oxidative and reductive peaks as in battery-type electrodes. In the first cycle of $\text{Ti}_2\text{C}_{0.5}\text{N}_{0.5}\text{T}_x$, an irreversible peak can be observed at 0.36 V. This peak disappeared in the following cycles, which relates to the electrolyte decomposition and the irreversible reaction of sodium with the surface terminations.^{30,62} In addition, the second and the third cycles are almost overlapping, indicating excellent reversibility of the electrochemical behavior. To further investigate the Na^+ storage mechanism, *ex situ* XRD was carried out after discharging to 0.001 V and charging back to 3 V versus Na/Na^+ . As shown in Figure S6, it is observed that the (002) peak

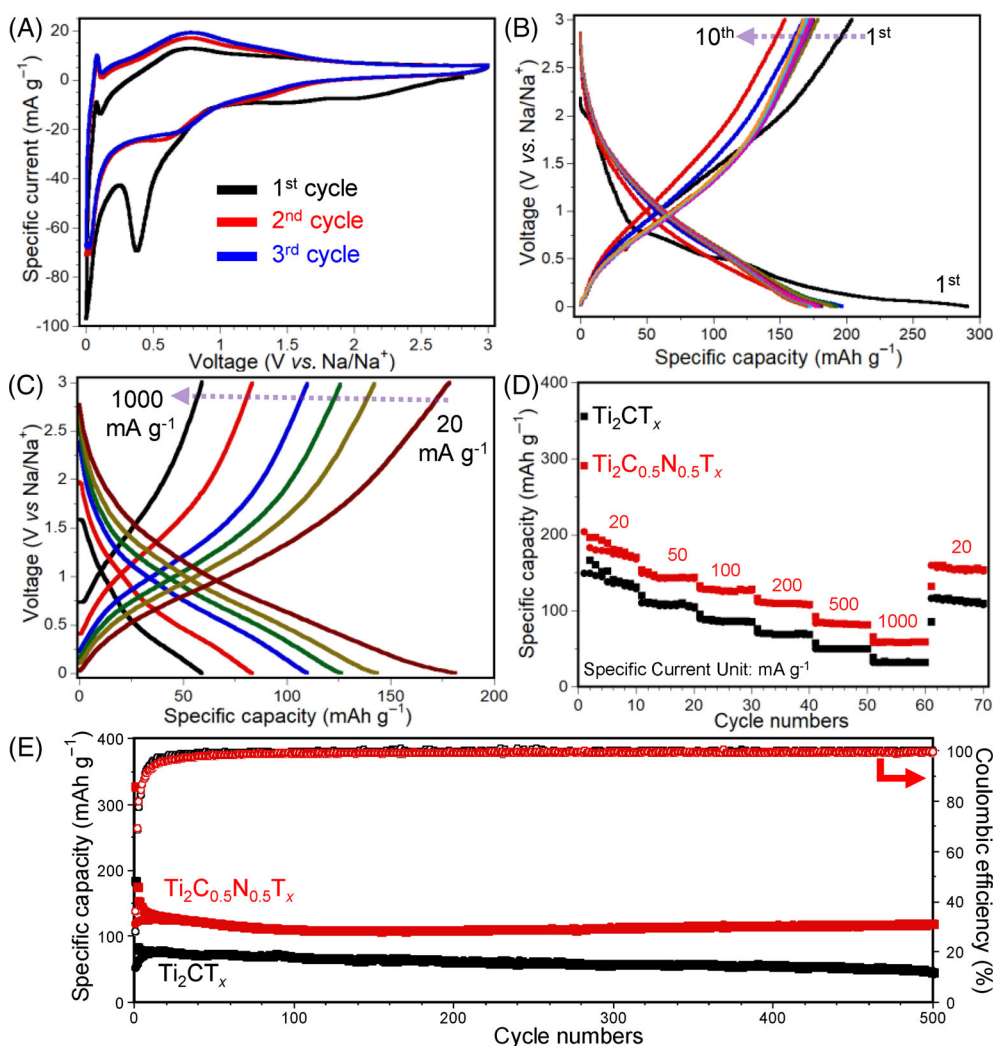


FIGURE 3 Electrochemical performance of $\text{Ti}_2\text{C}_{0.5}\text{N}_{0.5}\text{T}_x$ as a Na-ion battery electrode material. (A) CVs for the first 3 cycles at a scan rate of 0.1 mV s^{-1} . (B) First 10 cycles of galvanostatic charge/discharge testing at a specific current of 20 mA g^{-1} . (C) Galvanostatic charge/discharge profiles at different specific currents viz., 20, 50, 100, 200, 500, and 1000 mA g^{-1} . (D) Rate capabilities of $\text{Ti}_2\text{C}_{0.5}\text{N}_{0.5}\text{T}_x$ and Ti_2CT_x as Na-ion battery electrodes. (E) Long-term cycling performance at a current density of 200 mA g^{-1}

shifted to a slightly lower 2 theta angle, indicating the interlayer spacing was expanded after intercalating Na^+ by about 8.8%. This expansion in d -spacing upon sodiation and the fact that no new peaks were observed suggests an intercalation mechanism rather than a conversion reaction. A very small shift in the (002) peak to higher angle after charging back to 3 V (de-sodiation) can be observed. This suggests that some of the sodium form pillars between the layers maintaining the d -spacing at an almost constant value (in the range of 15.3–15.4 Å) during the electrochemical cycling, which leads to minimal volume change in the electrode and therefore enhances the stability.⁶⁵

Figure 3B shows the galvanostatic charge/discharge (GCD) voltage profiles for $\text{Ti}_2\text{C}_{0.5}\text{N}_{0.5}\text{T}_x$ at a specific current of 20 mA g^{-1} . The initial sodiation and de-sodiation specific capacities are 291 and 204 mAh g^{-1} , respectively, corresponding to a Coulombic efficiency of 70%. The specific capacity loss in the first sodiation and de-sodiation processes can be attributed to the solid electrolyte interphase layer formation below 0.9 V and other irreversible reactions between sodium and the MXene surface terminations. A reversible discharge capacity of 182 mAh g^{-1} was achieved after five cycles at 20 mA g^{-1} , which is larger than that of Ti_3CNT_x MXene and other MXenes as SIBs (for details, see Table S4).³⁰

To further investigate the electrochemical performance of $\text{Ti}_2\text{C}_{0.5}\text{N}_{0.5}\text{T}_x$ MXene, GCD tests were carried out at different specific currents. As shown in Figure 3C, no plateaus can be observed in the charge/discharge profiles, which agrees with CV results. Furthermore, the GCD curves show similar shapes, reflecting excellent reversibility of sodiation and de-sodiation processes. As displayed in Figure 3D, the specific capacity decreased to 142, 127, 109, 84, and 60 mAh g^{-1} when the specific currents increased to 50, 100, 200, 500, and 1000 mA g^{-1} , respectively. However, the specific capacity returned to 158 mAh g^{-1} when the specific current returned to

20 mA g^{-1} , demonstrating excellent rate handling capability and reversible sodiation and de-sodiation performance. $\text{Ti}_2\text{C}_{0.5}\text{N}_{0.5}\text{T}_x$ MXene shows 1.6–1.9 times higher specific capacity than Ti_2CT_x MXene, especially at high specific current, which suggests introducing N is promising for the development of high electrochemical performance electrode materials. As shown in Figure 3E, the as-prepared $\text{Ti}_2\text{C}_{0.5}\text{N}_{0.5}\text{T}_x$ MXene electrode exhibits excellent cycling performance at a specific current of 200 mA g^{-1} . The electrode shows a specific capacity of 112 mAh g^{-1} after 70 cycles. Moreover, the Coulombic efficiency of the electrode is around 98% after 40 cycles, reflecting a highly efficient electrochemical cycling. Moreover, after 500 cycles, we do not observe the capacity decay, reflecting high cycling stability. For comparison, Ti_2CT_x MXene electrode shows a stable specific capacity of 72 mAh g^{-1} before 200 cycles, after which the specific capacity decreases down to 46 mAh g^{-1} at 500 cycles.

Electrochemical impedance spectroscopy was conducted to investigate the kinetics of $\text{Ti}_2\text{C}_{0.5}\text{N}_{0.5}\text{T}_x$ MXene electrode. As shown in Figure 4A, Nyquist plots of $\text{Ti}_2\text{C}_{0.5}\text{N}_{0.5}\text{T}_x$ and Ti_2CT_x MXene electrodes display a semicircle from the high to medium frequency range and a straight line at low frequency range. It can be observed that $\text{Ti}_2\text{C}_{0.5}\text{N}_{0.5}\text{T}_x$ MXene electrode presents smaller system resistance of 5.8 Ω and charge-transfer resistance of 48.4 Ω than those of Ti_2CT_x MXene electrode (16.9 and 96.1 Ω , respectively).

As shown in Figure 4B, the Warburg factors of $\text{Ti}_2\text{C}_{0.5}\text{N}_{0.5}\text{T}_x$ and Ti_2CT_x MXene electrodes are 387.5 and 230, respectively, corresponding to the diffusion coefficients of 2.3×10^{-13} and 2.0×10^{-12} $\text{cm}^2 \text{s}^{-1}$ (for calculation details, see Supporting Information). These results reflect that the diffusivity of Na^+ is easier in Ti_2CT_x MXene electrodes than $\text{Ti}_2\text{C}_{0.5}\text{N}_{0.5}\text{T}_x$ MXene electrodes. This is because introducing N creates structural defects and different terminations.

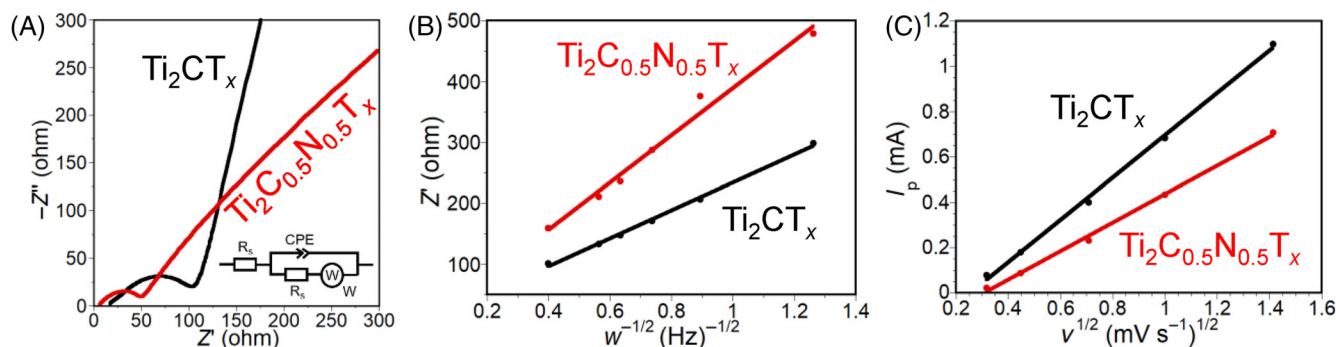


FIGURE 4 Dynamic analysis of $\text{Ti}_2\text{C}_{0.5}\text{N}_{0.5}\text{T}_x$ as Na-ion battery electrode. (A) Nyquist plots of $\text{Ti}_2\text{C}_{0.5}\text{N}_{0.5}\text{T}_x$ and Ti_2CT_x . (B) Randles plots of $\text{Ti}_2\text{C}_{0.5}\text{N}_{0.5}\text{T}_x$ and Ti_2CT_x . (C) Randles–Sevcik plots of $\text{Ti}_2\text{C}_{0.5}\text{N}_{0.5}\text{T}_x$ and Ti_2CT_x

To understand the higher Na⁺ capacity measured for Ti₂C_{0.5}N_{0.5}T_x MXene electrodes, the electroactive area of the electrode is calculated based on Randles–Sevcik equations⁶⁶:

$$I_p = (2.69 \times 10^5) n^{3/2} A_{\text{ea}} D^{1/2} \nu^{1/2} C \quad (1)$$

where n is the number of electrons transferred, A_{ea} is the electroactive area of the electrode, D is the diffusion coefficient, ν is the applied voltammetric scan rate, and C is the concentration of reaction. Figure S7 displays the CV curves at various scan rates of 0.1–2 mV s⁻¹. A pair of broad redox peaks at 0.7 and 0.85 V can be found, corresponding to Na⁺ intercalation and extraction from the Ti₂C_{0.5}N_{0.5}T_x MXene electrode.³³ As shown in Figure 4C, the electroactive area of the electrode can be calculated based on the fitting results of peak current and root of scan rate. The electroactive area of the electrodes of Ti₂C_{0.5}N_{0.5}T_x and Ti₂CT_x MXene electrodes are 7.1 and 3.2 m² g⁻¹, respectively, demonstrating that introducing N is an efficient way to increase the electroactive area of the electrodes to improve the electrochemical performance, which agrees with reported theoretical results.^{30,31,44} In addition, the slopes of peak currents for Ti₂CT_x and Ti₂C_{0.5}N_{0.5}T_x MXene electrodes in Figure 4C are 0.93 and 0.62, respectively, indicating that the control steps are a surface-controlled step and a diffusion-controlled step, which agrees with the large electroactive area of Ti₂C_{0.5}N_{0.5}T_x MXene electrode. Furthermore, the surface-controlled and diffusion-controlled portions can be calculated, as shown in Figures S8 and S9. The surface-controlled portion contributes 40% to the overall charge at 0.1 mV s⁻¹ and increases up to 72% at higher scan rates, as shown in Figure S8A. The predominant surface-controlled charge storage mechanism can afford ultrafast sodiation and de-sodiation processes, delivering high power density. Compared with Ti₂C_{0.5}N_{0.5}T_x MXene electrode, Ti₂CT_x shows a similar trend, as exhibited in Figure S8B.

The above discussion suggests that the advantages of introducing N into MXene systems can effectively maintain the favorable benefits of MXene systems for sodiation and de-sodiation processes, achieving high capacity and excellent rate handling capability for Na-ion storage. Introducing N into MXene systems also provides a high number of electroactive sites, leading to high capacity in SIBs. The importance of the present new carbonitride MXene goes beyond SIBs. Since Ti₃CNT_x were found to outperform Ti₃C₂T_x for many applications, such as electrodes for lithium and potassium ion batteries,^{30,67} catalysis,³⁹ and electromagnetic interference shielding.⁴⁰ Therefore, it is reasonable to predict that Ti₂C_{0.5}N_{0.5}T_x will find its way to other applications

beyond SIBs. More importantly, this work highlights the importance of exploring the role of X in MXenes for controlling MXene properties and performance.

3 | CONCLUSION

In summary, we report on the successful synthesis of a new 2D carbonitride MXene, *viz.*, Ti₂C_{0.5}N_{0.5}T_x, which is the only second carbonitride after Ti₃CNT_x in the large family of 40+ MXenes. The synthesis was carried out by etching Al from Ti₂AlC_{0.5}N_{0.5} using a mixture of HCl/KF, then delaminating with TMAOH treatment. Ti₂C_{0.5}N_{0.5}T_x MXene electrodes provide high electrical conductivity ($\sim 435 \pm 25$ S cm⁻¹), large electroactive surface area, and fast ion transport, showing a specific capacity of 182 mAh g⁻¹, the highest among all reported MXene electrodes in SIBs. In addition, the Ti₂C_{0.5}N_{0.5}T_x MXene electrode exhibits excellent long-term stability for 500 cycles. Our results suggest that developing transition metal carbonitrides is a promising approach to control and enhance the performance of MXenes.

ACKNOWLEDGMENTS

This work was supported as part of the Fluid Interface Reactions, Structures and Transport (FIRST) Center, an Energy Frontier Research Center funded by the U.S. Department of Energy, Office of Science, Office of Basic Energy Sciences. X-ray photoelectron spectroscopy measurement at the Molecular Foundry and X-ray absorption spectroscopy measurement at the Advanced Light Source were supported by the Office of Science, Office of Basic Energy Sciences, of the U.S. Department of Energy under Contract No. DE-AC02-05CH11231.

CONFLICT OF INTEREST

The authors declare no conflict of interest.

ORCID

Kun Liang  <https://orcid.org/0000-0001-5551-1439>
 Chaochao Dun  <https://orcid.org/0000-0002-3215-6478>
 Feipeng Yang  <https://orcid.org/0000-0002-5470-3241>
 Kaitlyn Prenger  <https://orcid.org/0000-0001-5654-2966>
 Michael Naguib  <https://orcid.org/0000-0002-4952-9023>

REFERENCES

1. Naguib M, Mochalin VN, Barsoum MW, Gogotsi Y. 25th anniversary article: MXenes: a new family of two-dimensional materials. *Adv Mater.* 2014;26(7):992-1005.
2. Naguib M, Mashtalir O, Carle J, et al. Two-dimensional transition metal carbides. *ACS Nano.* 2012;6(2):1322-1331.
3. Deysher G, Shuck CE, Hantanasirisakul K, et al. Synthesis of Mo₄AlC₄ MAX phase and two-dimensional Mo₄VC₄ MXene

- with five atomic layers of transition metals. *ACS Nano*. 2019;14(1):204-217.
- Naguib M, Kurtoglu M, Presser V, et al. Two-dimensional nanocrystals produced by exfoliation of Ti_3AlC_2 . *Adv Mater*. 2011;23(37):4248-4253.
 - Ghidiu M, Lukatskaya MR, Zhao MQ, Gogotsi Y, Barsoum MW. Conductive two-dimensional titanium carbide 'clay' with high volumetric capacitance. *Nature*. 2014;516(7529):78-81.
 - Husmann S, Budak Ö, Shim H, et al. Ionic liquid-based synthesis of MXene. *Chem Commun*. 2020;56(75):11082-11085.
 - Li M, Lu J, Luo K, et al. An element replacement approach by reaction with Lewis acidic molten salts to synthesize nanolaminated MAX phases and MXenes. *J Am Chem Soc*. 2019;141(11):4730-4737.
 - Gogotsi Y, Huang Q. MXenes: two-dimensional building blocks for future materials and devices. *ACS Nano*. 2021;15(4):5775-5780.
 - Zeraati AS, Mirkhani SA, Sun P, Naguib M, Braun PV, Sundararaj U. Improved synthesis of $\text{Ti}_3\text{C}_2\text{T}_x$ MXenes resulting in exceptional electrical conductivity, high synthesis yield, and enhanced capacitance. *Nanoscale*. 2021;13(6):3572-3580.
 - Firestein KL, von Treilfeldt JE, Kvashnin DG, et al. Young's modulus and tensile strength of Ti_3C_2 MXene nanosheets as revealed by in situ TEM probing, AFM nanomechanical mapping, and theoretical calculations. *Nano Lett*. 2020;20(8):5900-5908.
 - Anasori B, Lukatskaya MR, Gogotsi Y. 2D metal carbides and nitrides (MXenes) for energy storage. *Nat Rev Mater*. 2017;2:16098.
 - Guo L, Li Z, Marcus K, et al. Periodically patterned Au-TiO₂ heterostructures for photoelectrochemical sensor. *ACS Sens*. 2017;2(5):621-625.
 - Lukatskaya MR, Kota S, Lin Z, et al. Ultra-high-rate pseudocapacitive energy storage in two-dimensional transition metal carbides. *Nat Energy*. 2017;2(8):17105.
 - Xie Y, Naguib M, Mochalin VN, et al. Role of surface structure on Li-ion energy storage capacity of two-dimensional transition-metal carbides. *J Am Chem Soc*. 2014;136(17):6385-6394.
 - Kim SJ, Koh HJ, Ren CE, et al. Metallic $\text{Ti}_3\text{C}_2\text{T}_x$ MXene gas sensors with ultrahigh signal-to-noise ratio. *ACS Nano*. 2018;12(2):986-993.
 - Ding L, Wei Y, Wang Y, Chen H, Caro J, Wang H. A two-dimensional lamellar membrane: MXene nanosheet stacks. *Angew Chem*. 2017;129(7):1851-1855.
 - Khazaei M, Ranjbar A, Arai M, Sasaki T, Yunoki S. Electronic properties and applications of MXenes: a theoretical review. *J Mater Chem C*. 2017;5(10):2488-2503.
 - Li P, Zhu J, Handoko AD, et al. High-throughput theoretical optimization of the hydrogen evolution reaction on MXenes by transition metal modification. *J Mater Chem A*. 2018;6(10):4271-4278.
 - Seh ZW, Fredrickson KD, Anasori B, et al. Two-dimensional molybdenum carbide (MXene) as an efficient electrocatalyst for hydrogen evolution. *ACS Energy Lett*. 2016;1(3):589-594.
 - Rigby MTP, Natu V, Sokol M, et al. Synthesis of new M-layer solid-solution 312 max phases ($\text{Ta}_{1-x}\text{Ti}_x$)₃AlC₂ (X = 0.4, 0.62, 0.75, 0.91 or 0.95), and their corresponding MXenes. *RSC Adv*. 2021;11(5):3110-3114.
 - Pinto D, Anasori B, Avireddy H, et al. Synthesis and electrochemical properties of 2d molybdenum vanadium carbides—solid solution MXenes. *J Mater Chem A*. 2020;8(18):8957-8968.
 - Han M, Maleski K, Shuck CE, et al. Tailoring electronic and optical properties of MXenes through forming solid solutions. *J Am Chem Soc*. 2020;142(45):19110-19118.
 - Yang J, Naguib M, Ghidiu M, et al. Two-dimensional Nb-based M_4C_3 solid solutions (MXenes). *J Am Ceram Soc*. 2016;99(2):660-666.
 - Nemani SK, Zhang B, Wyatt BC, et al. High-entropy 2D carbide MXenes: TiVNbMoC_3 and TiVCrMoC_3 . *ACS Nano*. 2021;15(8):12815-12825.
 - Kamysbayev V, Filatov AS, Hu H, et al. Covalent surface modifications and superconductivity of two-dimensional metal carbide MXenes. *Science*. 2020;369(6506):979-983.
 - Li Y, Shao H, Lin Z, et al. A General Lewis acidic etching route for preparing MXenes with enhanced electrochemical performance in non-aqueous electrolyte. *Nat Mater*. 2020;19(8):894-899.
 - Naguib M, Barsoum MW, Gogotsi Y. Ten years of progress in the synthesis and development of MXenes. *Adv Mater*. 2021;33(39):2103393.
 - Liang X, Rangom Y, Kwok CY, Pang Q, Nazar LF. Interwoven MXene nanosheet/carbon-nanotube composites as Li-S cathode hosts. *Adv Mater*. 2017;29:1603040.
 - Zhang C, Kremer MP, Seral-Ascaso A, et al. Stamping of flexible, coplanar micro-supercapacitors using MXene inks. *Adv Funct Mater*. 2018;28:1705506.
 - Zhu J, Wang M, Lyu M, et al. Two-dimensional titanium carbonitride MXene for high-performance sodium ion batteries. *ACS Appl Nano Mater*. 2018;1(12):6854-6863.
 - Zhang W, Liu S, Chen J, et al. Exploring the potentials of $\text{Ti}_3\text{C}_i\text{N}_{2-i}\text{T}_x$ (i=0, 1, 2)-MXene for anode materials of high-performance sodium-ion batteries. *ACS Appl Mater Interfaces*. 2021;13(19):22341-22350.
 - Zhang CJ, Park SH, Seral-Ascaso A, et al. High capacity silicon anodes enabled by MXene viscous aqueous ink. *Nat Commun*. 2019;10(1):1-9.
 - Wang X, Shen X, Gao Y, Wang Z, Yu R, Chen L. Atomic-scale recognition of surface structure and intercalation mechanism of $\text{Ti}_3\text{C}_2\text{X}$. *J Am Chem Soc*. 2015;137(7):2715-2721.
 - Jhon YI, Koo J, Anasori B, et al. Metallic MXene saturable absorber for femtosecond mode-locked lasers. *Adv Mater*. 2017;29:1702496.
 - Hantanasirisakul K, Alhabeb M, Lipatov A, et al. Effects of synthesis and processing on optoelectronic properties of titanium carbonitride MXene. *Chem Mater*. 2019;31(8):2941-2951.
 - Jin Z, Li P, Xiao D. Enhanced electrocatalytic performance for oxygen reduction via active interfaces of layer-by-layered titanium nitride/titanium carbonitride structures. *Sci Rep*. 2014;4(1):1-7.
 - Roca-Ayats M, Herreros E, García G, Pena M, Martínez-Huerta M. Promotion of oxygen reduction and water oxidation at Pt-based electrocatalysts by titanium carbonitride. *Appl Catal B*. 2016;183:53-60.
 - Roca-Ayats M, Guillén-Villafuerte O, García G, Soler-Vicedo M, Pastor E, Martínez-Huerta M. PtSn nanoparticles supported on titanium carbonitride for the ethanol oxidation reaction. *Appl Catal B*. 2018;237:382-391.

39. Naguib M, Tang W, Browning KL, et al. Catalytic activity of Ti-based MXenes for the hydrogenation of furfural. *ChemCatChem*. 2020;12(22):5733-5742.
40. Iqbal A, Shahzad F, Hantanasirisakul K, et al. Anomalous absorption of electromagnetic waves by 2D transition metal carbonitride Ti_3CNT_x (MXene). *Science*. 2020;369(6502):446-450.
41. Hong X, Wang Q, Tang Z, Khan W, Zhou D, Feng T. Synthesis and electromagnetic absorbing properties of titanium carbonitride with quantificational carbon doping. *J Phys Chem C*. 2016;120(1):148-156.
42. Huang S, Mochalin VN. Understanding chemistry of two-dimensional transition metal carbides and carbonitrides (MXenes) with gas analysis. *ACS Nano*. 2020;14(8):10251-10257.
43. Yang T, Gao L, Wang W. Berlin green framework-based gas sensor for room-temperature and high-selectivity detection of ammonia. *Nano-Micro Lett*. 2021;13(1):1-13.
44. Guo W, She Z, Xue H, Zhang X. Density functional theory study on the Ti_3CN and Ti_3CNT_2 (T=O, S and F) as high capacity anode material for Na ion batteries. *Appl Surf Sci*. 2020;529:147180.
45. Wang X, Kajiyama S, Iinuma H, et al. Pseudocapacitance of MXene nanosheets for high-power sodium-ion hybrid capacitors. *Nat Commun*. 2015;6(1):1-6.
46. Xie Y, Dall'Agnese Y, Naguib M, et al. Prediction and characterization of MXene nanosheet anodes for non-lithium-ion batteries. *ACS Nano*. 2014;8(9):9606-9615.
47. Surucu G, Erkisi A. The first principles investigation of structural, electronic, mechanical and lattice dynamical properties of the B and N doped M_2AX type MAX phases $Ti_2AlB_{0.5}C_{0.5}$ and $Ti_2AlN_{0.5}C_{0.5}$ compounds. *J Boron*. 2018;3(1):24-32.
48. Shein IR, Ivanovskii AL. Graphene-like titanium carbides and nitrides $Ti_{n+1}C_n$, $Ti_{n+1}N_n$ ($n=1, 2$, and 3) from de-intercalated MAX phases: first-principles probing of their structural, electronic properties and relative stability. *Comput Mater Sci*. 2012;65:104-114.
49. Abdelmalak MN. *MXenes: a New Family of Two-Dimensional Materials and its Application as Electrodes for Li-Ion Batteries*. Philadelphia, PA: Drexel University; 2014.
50. Barsoum M, El-Raghy T, Ali M. Processing and characterization of Ti_2AlC , Ti_2AlN , and $Ti_2AlC_{0.5}N_{0.5}$. *Metall Mater Trans A*. 2000;31(7):1857-1865.
51. Ud Din MF, Yang C, Tang Y, et al. Efficient and cost-effective method to synthesize highly purified Ti_4AlN_3 and Ti_2AlN . *J Adv Dielectr*. 2019;9(01):1950008.
52. Alhabeab M, Maleski K, Mathis TS, et al. Selective etching of silicon from Ti_3SiC_2 (MAX) to obtain 2D titanium carbide (MXene). *Angew Chem Int Ed*. 2018;57(19):5444-5448.
53. Sun W, Wang HW, Vlcek L, et al. Multiscale and multimodal characterization of 2D titanium carbonitride MXene. *Adv Mater Interfaces*. 2020;7(11):1902207.
54. Ghidiu M, Naguib M, Shi C, et al. Synthesis and characterization of two-dimensional Nb_4C_3 (MXene). *Chem Commun*. 2014;50(67):9517-9520.
55. Naguib M, Unocic RR, Armstrong BL, Nanda J. Large-scale delamination of multi-layers transition metal carbides and carbonitrides "MXenes". *Dalton Trans*. 2015;44(20):9353-9358.
56. Mashtalir O, Naguib M, Mochalin VN, et al. Intercalation and delamination of layered carbides and carbonitrides. *Nat Commun*. 2013;4(1):1-7.
57. Hu T, Yang J, Li W, Wang X, Li CM. Quantifying the rigidity of 2D carbides (MXenes). *Phys Chem Chem Phys*. 2020;22(4):2115-2121.
58. Ying G, Dillon AD, Fafarman AT, Barsoum MW. Transparent, conductive solution processed spincast 2D Ti_2CT_x (MXene) films. *Materials Research Letters*. 2017;5(6):391-398.
59. Du F, Tang H, Pan L, et al. Environmental friendly scalable production of colloidal 2D titanium carbonitride MXene with minimized nanosheets restacking for excellent cycle life lithium-ion batteries. *Electrochim Acta*. 2017;235:690-699.
60. Halim J, Cook KM, Naguib M, et al. X-ray photoelectron spectroscopy of select multi-layered transition metal carbides (MXenes). *Appl Surf Sci*. 2016;362:406-417.
61. Natu V, Pai R, Sokol M, Carey M, Kalra V, Barsoum MW. 2D $Ti_3C_2T_z$ MXene synthesized by water-free etching of Ti_3AlC_2 in polar organic solvents. *Chem*. 2020;6(3):616-630.
62. Kajiyama S, Szabova L, Sodeyama K, et al. Sodium-ion intercalation mechanism in Mxene nanosheets. *ACS Nano*. 2016;10(3):3334-3341.
63. Xie X, Kretschmer K, Anasori B, Sun B, Wang G, Gogotsi Y. Porous $Ti_3C_2T_x$ MXene for ultrahigh-rate sodium-ion storage with long cycle life. *ACS Appl Nano Mater*. 2018;1(2):505-511.
64. Anayee M, Kurra N, Alhabeab M, et al. Role of acid mixtures etching on the surface chemistry and sodium ion storage in $Ti_3C_2T_x$ MXene. *Chem Commun*. 2020;56(45):6090-6093.
65. Ye H, Zhang Y, Yin Y-X, Cao F-F, Guo Y-G. An outlook on low-volume-change lithium metal anodes for long-life batteries. *ACS Central Sci*. 2020;6(5):661-671.
66. Liang K, Marcus K, Zhang S, et al. NiS_2/FeS holey film as free-standing electrode for high-performance lithium battery. *Adv Energy Mater*. 2017;7:1701309.
67. Naguib M, Adams RA, Zhao Y, et al. Electrochemical performance of Mxenes as K-ion battery anodes. *Chem Commun*. 2017;53(51):6883-6886.

SUPPORTING INFORMATION

Additional supporting information may be found in the online version of the article at the publisher's website.

How to cite this article: Liang K, Tabassum A, Majed A, et al. Synthesis of new two-dimensional titanium carbonitride $Ti_2C_{0.5}N_{0.5}T_x$ MXene and its performance as an electrode material for sodium-ion battery. *InfoMat*. 2021;3(12):1422-1430. <https://doi.org/10.1002/inf2.12269>